CHAPTER 7

INCORPORATION AND TRANSPORT OF DOPANTS

7.1 INTRODUCTION

Incorporation of dopants into a semiconductor material, commonly referred to as doping, is the means by which junctions are formed and is essentially what makes a semiconductor function as an integrated circuit. Thermal diffusion and ion implantation are the methods used to introduce a controlled amount of chosen impurities (dopants) into selected regions of a semiconductor. The more recent method of ion implantation is often preferred because of its capability to control the number of implanted dopant atoms. For silicon, for example, precise dopant concentrations can be obtained from 10^{14} to 10^{21} atoms/cm^3.

Dopant incorporation by thermal diffusion usually involves a two-step processing of predeposition followed by "drive-in." Predeposition is a process in which a dopant in the gas phase is introduced into the semiconductor by being in contact with the solid surface at high temperature. Since the dopant concentration in the gas phase is kept constant, the solid surface becomes saturated with the dopant atom to the solid solubility, while surface dopant atoms diffuse into the solid interior. This predeposition is followed by drive-in in which the semiconductor is heated in an inert environment to cause a redistribution of the predeposited dopant to a desired dopant profile.

There are three different ways of carrying out the predeposition. The first, shown in Fig. 7-1, involves introducing a dopant-carrying gas stream to a furnace

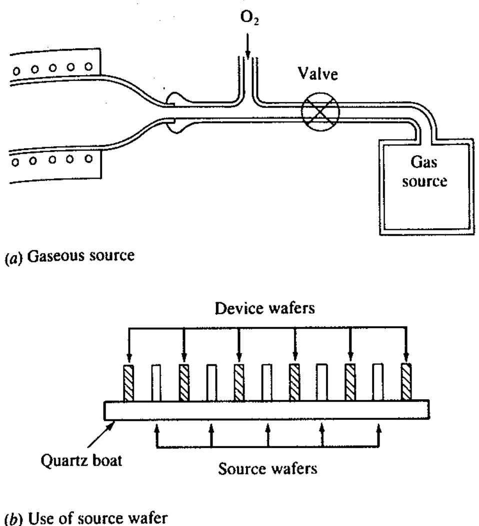

FIGURE 7-1
Predeposition methods (Gise and Blanchard, 1979).

containing a quartz boat on which wafers are stacked upright as in the LPCVD reactor. Although Fig. 7-1*a* only shows a gas dopant source, the dopant source can also be solid or liquid. Chemical reaction between the carrier gas (usually nitrogen) and the solid source produces the dopant when the source is solid. For liquid sources, a carrier gas bubbled through a liquid compound containing the dopant produces a wet gas stream saturated with the dopant. In most cases, oxygen is added to the gas flow to ensure that the dopant reaches the wafer surface as an oxide. Another method uses wafers made of a compound of the desired dopant. These source wafers are usually prepared by oxidizing them. They are placed as shown in Fig. 7-1*b* in a quartz boat and then introduced to a furnace. An inert gas is used for the predeposition. The third method involves the use of a doped layer of an oxide such as silicon dioxide (for silicon wafers) that is bonded to the wafer surface. This can be accomplished by depositing a doped layer of oxide by a low-temperature CVD process or by bonding a doped layer to the wafer surface by a spinning-on technique, in much the same way as the spinning-on coating of a photoresist. The wafers are loaded into a furnace with the dopant layer already on the front side of the wafer. During the predeposition, the required amount of dopant diffuses into the semiconductor.

Masking against dopant diffusion is usually accomplished with silicon dioxide. Only the area not masked is involved in the predeposition. The thickness required to mask against the diffusion is dependent on the type of dopant, time, and temperature, but is usually less than 1 μm. The drive-in is carried out in an oxidizing atmosphere to regrow a protective oxide layer over the freshly diffused region.

Ion implantation offers a number of technological advantages such as speed and reproducibility of the doping process, and exact controllability of the number of doping atoms introduced. It is particularly useful for forming shallow junctions with high doping requirements. In ion implantation, ionized-projectile atoms are introduced into solid targets with enough kinetic energy (3 to 500 keV) to penetrate beyond the surface regions, anywhere from 100 angstroms up to micrometers. The high energy used is perhaps the main distinction between ion implantation and particle (particularly ion) beam lithography (treated in Chap. 8). A schematic of a typical commercial ion implant system is shown in Fig. 7-2. As shown, a gas source of dopant such as BF_3 or AsH_3 is energized at a high potential to produce an ion plasma, containing dopant ions. The analyzer magnet then selects only the ion species of interest and rejects other species. The desired ion species is then injected to the accelerator through a revolving slit, where its velocity is increased. The x- and y-scan plates direct the beam to the target wafers. The wafer feeding arrangement (denoted simply as wafer in Fig. 7-2) is external to the whole machine in one package such that wafers can be loaded and unloaded through a feeder. Because of the nature of ion implantation, the implantation is basically independent of solid solubility limits, temperature during implantation, and concentration of dopant at the semiconductor surface. The doping atoms introduced have a concentration profile that is generally described by a Gaussian distribution. Although ion implantation in this chapter is treated only in relation to doping, it is not difficult to imagine other various

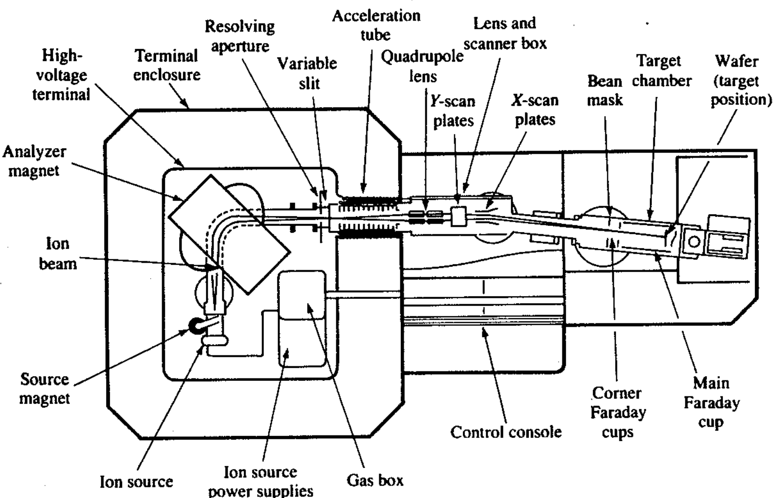

FIGURE 7-2
Schematic illustration of a medium current implanter (Ryssel and Ruge, 1986).

applications. One example is the current practice of forming an insulator below the semiconductor surface by deeply implanting oxygen ions and then annealing.

Ion implantation, however, does have its problems. Because of the bombardment involved with heavy particles, radiation damage occurs, which in turn causes changes in the electrical properties of semiconductor. The radiation damage is the major problem with ion implantation. Most of the doping atoms do not come to rest after implantation on regular lattice sites, and are therefore not electrically active. By a suitable annealing method, the crystal lattice is restored and the introduced dopant atoms brought to electrically active lattice sites by diffusion. Side effects of implantation such as ion channeling are another source of problems.

Both thermal diffusion and ion implantation methods involve diffusion of dopant atoms in the semiconductor during and after dopant incorporation. Therefore, the nature of diffusion will be examined first before considering the subject of dopant incorporation.

7.2 NATURE OF DIFFUSION IN SOLIDS

Diffusion in solids can be visualized as movement of atoms through vacancies and interstitial regions of the crystal lattice. Lattice atoms vibrate around their equilibrium sites in much the same way as in the case of surface diffusion considered in Chap. 5. As the temperature is raised, some lattice atoms occasionally acquire sufficient energy to overcome the binding energy and leave the lattice sites, thereby creating lattice vacancies and interstitials, shown in Fig. 7-3. When a neighboring host or impurity atom migrates to the vacancy site, the diffusion is referred to as diffusion by the vacancy mechanism. When an interstitial atom

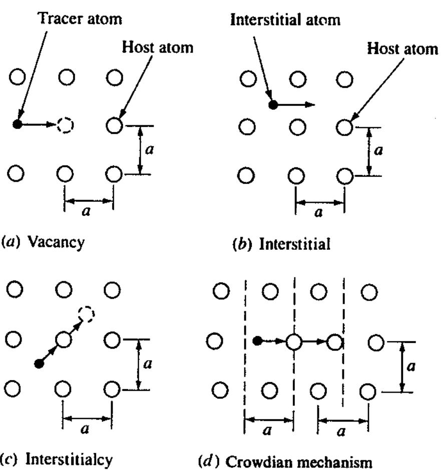

FIGURE 7-3
Models of diffusion mechanism with a the lattice constant (Tuck, 1974).

moves from one interstitial site to another without occupying a lattice site, interstitial diffusion is said to have taken place. Extensions of interstitial diffusion are also shown in Fig. 7-3, which involve simultaneous movement of two atoms. Diffusion is called self-diffusion or impurity diffusion depending on whether a migrating atom is a host or impurity atom.

Because of smaller binding energy associated with interstitial atoms, the activation energy required for diffusion of interstitial atoms is lower than for diffusion of lattice atoms via the vacancy mechanism. An atom smaller than the host atom often moves interstitially. Group I and VIII elements have small ionic radii compared with silicon. They diffuse fast in silicon and they are considered to diffuse by an interstitial mechanism. On the other hand, group III and V elements are considered to diffuse predominantly by the vacancy mechanism. They are slow diffusers. Diffusion in gallium arsenide is believed to take place by movement on sublattices, i.e., the gallium sublattice and arsenic sublattice. Group II elements, which are p type, are believed to move along the gallium sublattice by interstitial mechanisms. Group VI elements, which are n type, are believed to move along the arsenic sublattice by the vacancy mechanism. They are slow diffusers. Group IV elements, which can be either n or p type depending on the sublattice on which they are preferentially located, are usually assumed to move on both sublattices. They are extremely slow diffusers.

As was the case in surface diffusion, the flux of atoms J in solid can also be described by Fick's law:

$$J = -D \frac{\partial C}{\partial x} \tag{7.1}$$

where D is the diffusivity and C is the concentration. Because of the impurities (dopant atoms) present in a semiconductor, diffusion and thus the diffusivity depends strongly on the impurity content in the solid. For intrinsic semiconductors (those with an impurity concentration less than the intrinsic carrier concentration n_i), the impurity effect is negligible and the diffusivity can be considered as that of the intrinsic material. This intrinsic diffusivity D_i can be expressed as follows:

$$D_i = D_0 \exp\left(-\frac{E}{k_B T}\right) \tag{7.2}$$

where D_0 is the preexponential factor dependent on the vibrational frequency of atoms in lattice or interstitial sites and E is the binding energy at the site.

Point defects such as vacancies and interstitial atoms play a dominant role in the diffusion of impurities in semiconductors (Boltaks, 1963; Frank *et al.*, 1984) along with the charge state of the point defects. A vacancy or an interstitial atom can be neutral or charged by exchanging electrons. Thus, a point defect can be neutral, which is called a neutral point defect, or negatively (acceptor point defect) or positively (donor point defect) charged. Even for intrinsic semiconductors, a distinction is made as to which type of point defect dominates the diffusion. Because of the extensive work available for silicon, the intrinsic diffusi-

TABLE 7.1
Intrinsic diffusivity of B, P, As, and Sb (Fair, 1981)

Unit	B(D_i^+)	P($D_i^\times$)	As(D_i^-)	Sb($D_i^\times$)
D_0, cm²/s	0.76	3.85	22.9	0.214
E, eV	3.46	3.66	4.10	3.65

vities are denoted by $D_i^\times$ (neutral), D_i^- (acceptor point effect), and D_i^+ (donor point defect) to signify the dominance of a particular type of point defect in the diffusion. The diffusivities are given in Table 7.1. For gallium arsenide, however, less information is available for the various types of diffusion. The diffusivities are summarized in Table 7.2.

Diffusivity is usually defined as the root mean square distance an atom travels per unit time (Sec. 5.2). If one assigns parts of the distance travelled to the distance due to neutral point defects and that due to charged point defects, one has

$$D_i = D_i^\times + D_i^+ + D_i^- + D_i^{2-} + \cdots \tag{7.3}$$

Under extrinsic conditions, however, the concentration of various point defects changes due to the excess amount of impurities. The neutral point defect concentration should remain the same, since it is not affected by the electric field induced by the impurity concentration gradient. Since diffusion is the movement of impurity atoms along point defects, the diffusivity, or the distance travelled, should be weighted according to the change in the point defects' concentrations when excessive impurity atoms are present (Shaw, 1973). Thus, one has

$$D = D_i^\times + D_i^+ \frac{[\mathrm{P}^+]}{[\mathrm{P}^+]_i} + D_i^- \frac{[\mathrm{P}^-]}{[\mathrm{P}^-]_i} + D_i^{2-} \frac{[\mathrm{P}^{2-}]}{[\mathrm{P}^{2-}]_i} + \cdots \tag{7.4}$$

TABLE 7.2
Diffusivities of impurities in GaAs (Shaw, 1973)

Impurity	D_0, cm²/s	E, eV
Au	2.9×10^1	2.64
Be	7.3×10^{-6}	1.2
Cr	4.3×10^3	3.4
Cu	3×10^{-2}	0.53
Li	5.3×10^{-1}	1.0
Mg	2.6×10^{-2}	2.7
Mn	6.5×10^{-1}	2.49
O	2×10^{-3}	1.1
S	1.85×10^{-2}	2.6
Se	3.0×10^3	4.16
Sn	3.8×10^{-2}	2.7

where it has been recognized that $[P^\times]_i = [P^\times]$. The point defects' concentrations are denoted by brackets and the subscript i is used to designate the intrinsic semiconductor. For charged point defects, one has

$$P^\times + re^- \rightleftharpoons P^{-r} \tag{7.5}$$

At equilibrium, one can write

$$K_r = \frac{[P^{-r}]_i}{n_i^r[P^\times]}$$

where n_i is the intrinsic carrier concentration. Under intrinsic conditions, $p = p_i = n_i$ such that

$$K_r = \frac{[P^{-r}]_i}{n_i^r[P^\times]_i}$$

Combining the two equations yields

$$\frac{[P^{-r}]}{[P^{-r}]_i} = \left(\frac{n}{n_i}\right)^r \tag{7.6}$$

since $[P^\times]_i = [P^\times]$. Similar expressions can be obtained for different charged point defects. Using Eq. (7.6) and the similar expressions in Eq. (7.5) gives

$$D = D_i^\times + D_i^+\left(\frac{p}{n_i}\right) + D_i^-\left(\frac{n}{n_i}\right) + D_i^{2-}\left(\frac{n}{n_i}\right)^2 + \cdots \tag{7.7}$$

Example 7.1. For silicon, the bandgap energy E_g varies from about 1.11 eV at 300 K to about 1.16 eV at 0 K. Neglecting this change and also the $T^{3/2}$ dependence, the temperature dependence of intrinsic carrier concentration for any semiconductor is approximately given by

$$\frac{n_i(T)}{n_i(300)} = \exp\left[-\frac{E_g}{2k}\left(\frac{1}{T} - \frac{1}{300}\right)\right]$$

For silicon at 300 K, $n_i = 1.5 \times 10^{10}$ cm^{-3}. As shown in Table 7.1, the diffusion of boron in silicon is dominated by acceptor point defects. Calculate the boron diffusivity at 1000 K in silicon doped with boron at 10^{17} cm^{-3}.

Solution. If the acceptor point defect dominates, Eq. (7.7) reduces to

$$D = D_i^+\left(\frac{p}{n_i}\right)$$

$$= \left[0.76 \exp\left(-\frac{3.46}{k_B T}\right)\right]\left(\frac{10^{17}}{1.5 \times 10^{10}}\right)$$

$$= 0.76 \exp\left[-\frac{3.46}{(8.63 \times 10^{-5})(1000)}\right]\left(\frac{10^7}{1.5}\right)$$

$$= 1.96 \times 10^{-11} \text{ cm}^2/\text{s}$$

An effect much less important than impurity effects is the enhancement of diffusion by the electric field between the impurity atoms ionized at diffusion

temperature and the electrons and holes (Hu and Schmidt, 1968). For an n-type impurity as an example, the flux in one dimension is given by

$$J = -D\frac{dN}{dx} + \mu n E \tag{7.8}$$

where N is the impurity concentration, μ is the electron mobility, and E is the electric field. Using the Einstein relationship and

$$E = -\frac{k_B T}{q}\frac{1}{n}\frac{dn}{dx} \tag{7.9}$$

one has

$$J = -D\left(1 + \frac{dn}{dN}\right)\frac{dN}{dx}$$

$$= -Dh\frac{dN}{dx} \tag{7.10}$$

where $h = 1 + dn/dN$ is the field enhancement factor. For an n-type impurity, one has

$$\frac{n}{n_i} = \frac{N}{2n_i} + \left[\left(\frac{N}{2n_i}\right)^2 + 1\right]^{\frac{1}{2}} \tag{7.11}$$

such that

$$\frac{dn}{dN} = \frac{1}{2}\left\{1 + \left[1 + \left(\frac{2n_i}{N}\right)^2\right]^{-1/2}\right\} \tag{7.12}$$

It can be seen that dn/dN approaches unity as N or the impurity concentration becomes much larger than n_i. Therefore, the maximum value of h is 2. Note that the same relationship holds for a p-type semiconductor if n is replaced by p. In general, then, the diffusivity can be expressed as follows:

$$D = h\left[D_i^\times + D_i^+\left(\frac{p}{n_i}\right) + D_i^-\left(\frac{n}{n_i}\right) + D_i^{2-}\left(\frac{n}{n_i}\right)^2 + \cdots\right] \tag{7.13}$$

An oxidizing environment significantly affects diffusion. As discussed in the previous section, doping by thermal diffusion is often carried out in the presence of oxygen, particularly during the drive-in step. This serves the dual purpose of providing an oxide layer for the next photoengraving process and creating steps in the surface of the silicon wafer, since the oxide growth rate in the window area is much greater than that under the already oxidized regions, permitting alignment of patterns. The diffusivity under oxidizing environment is often correlated (Taniguchi *et al.*, 1980; Lin *et al.*, 1981) as follows:

$$D_m = D_i + \Delta D \tag{7.14}$$

$$\Delta D = \alpha\left(\frac{dX}{dt}\right)^n \tag{7.15}$$

where D_m is the diffusivity as modified by the presence of oxygen, ΔD is the corresponding change under oxidizing conditions, α is a proportionality constant, the exponent n is between 0.4 and 0.6, and dX/dt is the oxidation rate. Another enhancement (sometimes retardation) effect is lateral enhanced diffusion (Kennedy and O'Brien, 1965; Gibbon *et al.*, 1972) at an oxide or silicon-nitride edge. Elastic strain of the lattice near the window "edges" has been cited as the reason for the enhancement.

Diffusion of impurities in polycrystalline materials is also of interest in microelectronics processing. A case in point is the doping of polycrystalline silicon used as a gate material. Because the least resistance to diffusion is along grain boundaries, the overall diffusivity is higher than the diffusivity in a single crystal and depends heavily on the grain structure. Nevertheless, a single diffusivity can be assigned to a given material to estimate the dopant distribution. Typical diffusivities are in the range of 10^{-13} to 10^{-14} cm^2/s (Tsai, 1983).

Diffusion in silicon oxide is also of interest, since it is used as a mask against impurity diffusion. As might be expected from the fact that it is used as a mask, the diffusivities are much lower in silicon oxide than in silicon. Diffusivities of various elements in silicon oxide are given in Table 7.3 along with those in silicon for some of the elements.

7.3 DOPANT INCORPORATION

Two different methods can be used to introduce a dopant into a semiconductor. These are thermal diffusion and ion implantation. The diffusion process alone is sufficient to analyze doping by thermal diffusion. On the other hand, some basics of ion beams and its scattering in solids have to be understood before doping by ion implantation can be understood.

Consider the doping by thermal diffusion discussed in Sec. 7.1 which involved a two-step process to obtain a desired dopant profile. During predeposition, the semiconductor is either exposed to a gas stream containing excess dopant at low temperature in order to obtain a surface region saturated with the dopant or a dopant is diffused into a thin surface layer from a solid dopant source coated onto the semiconductor surface. In the drive-in step, the dopant in the thin surface layer of the semiconductor is diffused into the interior at high temperature to obtain the desired dopant profile. Regardless of the steps, therefore, the problem of determining the profile reduces to two different cases, either diffusion with constant surface concentration or diffusion with constant total dopant present. Thermal diffusion for gallium arsenide is often carried out with doped cap layers of oxides (e.g., Ghandhi and Field, 1981) to inhibit arsenic evaporation at the doping temperature.

TABLE 7.3
Diffusivities of various elements in SiO_2 and Si (Tsai, 1983)

	SiO_2		Si	
Element	D_0, cm^2/s	E, eV	D_0, cm^2/s	E, eV
B	7.23×10^{-6}	2.38	—	
Ga	1.04×10^{5}	4.17	—	
P	5.73×10^{-5}	2.30	—	
As	67.25	4.7	—	
Sb	1.31×10^{16}	8.75	—	
Au	8.2×10^{-10}	0.8	1.1×10^{-3}	1.12
Pt	1.2×10^{-13}	0.75	1.6×10^{2}	2.18
Na	6.9	1.3	1.6×10^{-3}	0.76

The thickness of the doped layer is small such that a one-dimensional conservation equation in the direction perpendicular to the surface, x, can be used. For this one-dimensional case, one has

$$\frac{\partial C}{\partial t} = -\frac{\partial J}{\partial x} = \frac{\partial}{\partial x}\left(D\,\frac{\partial C}{\partial x}\right) \tag{7.16}$$

where Eq. (7.1) has been used. For the constant surface concentration case, the semiconductor surface is saturated with the dopant from the gas phase. Thus, one of the boundary conditions is

$$C(0, t) = C_s \tag{7.17}$$

where C_s is the saturation concentration. Far away from the surface, the dopant concentration is zero, i.e., $C(\infty, t) = 0$. Also, there is no dopant initially in the solid, i.e., $C(x, 0) = 0$. The solution of Eq. (7.17) with the initial and boundary conditions is

$$C(x, t) = C_s \operatorname{erfc}\left[\frac{x}{(4Dt)^{1/2}}\right] \tag{7.18}$$

where the diffusivity has been assumed to be constant. The complementary error function, erfc $(y) = 1 - \operatorname{erf}(y)$, is a tabulated function and can be found in the Appendix.

For the constant total dopant case, the only difference is in one of the boundary conditions, which is

$$\int_0^\infty C(x, t)\, dx = Q_o \tag{7.19}$$

where Q_o is the total amount of dopant initially present per unit exposed area. In the case of predeposition followed by drive-in, Q_o is the amount predeposited per unit area. The solution of Eq. (7.16) for this case is

$$C(x, t) = \frac{Q_o}{(\pi D t)^{1/2}} \exp\left(-\frac{x^2}{4Dt}\right) \tag{7.20}$$

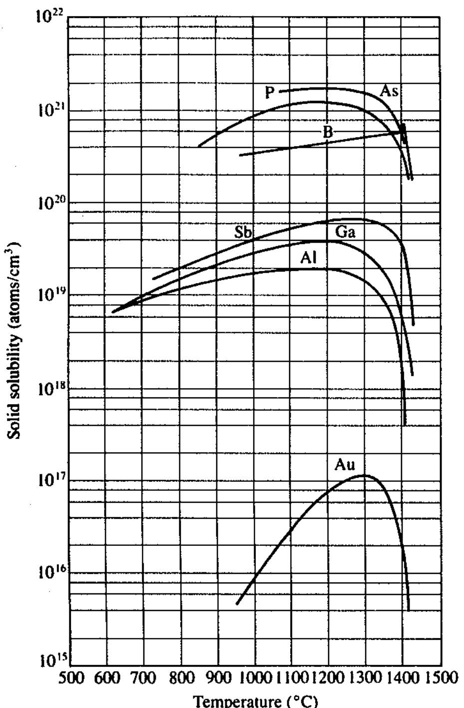

FIGURE 7-4
Solid solubility of dopants in silicon (Gise and Blanchard, 1979).

When Q_o is the amount resulting from predeposition, its value can be obtained by

$$Q_o = 2C_s\left(\frac{D_1 t_1}{\pi}\right)^{1/2} \tag{7.21}$$

where the subscript 1 is for predeposition values.

The saturation solid solubility C_s is relatively well known for impurities in silicon. The solubility curves are shown in Fig. 7-4 as a function of temperature. As seen from the figure, the solubilities in general increase with temperature, reach a maximum, and fall off rapidly as the melting point of the host material, which is silicon in this case, is approached. This behavior is commonly referred to as retrograde solid solubility characteristics.

Example 7.2. A predeposition is carried out for 15 minutes for an n-type silicon wafer (10^{17} atoms/cm^3) at 950 °C using a gas containing excess boron. Determine the junction depth and the distance from the surface at which the dopant concentration is one half of the surface saturation concentration. At 950 °C, the saturation concentration is 3.8×10^{20} atoms/cm^3.

Solution. The junction depth is determined by the point of transition from p-type to n-type silicon. Therefore, the junction depth x_j is determined from

$$C_s \operatorname{erfc}\left[\frac{x_j}{(4Dt)^{1/2}}\right] = 10^{17} \tag{A}$$

where Eq. (7.18) has been used. For boron, the diffusivity (Table 7.1) is given by

$$D = 0.76 \exp\left(-\frac{3.46}{k_B T}\right)$$
$$= 0.76 \exp\left[-\frac{3.46}{(8.36 \times 10^{-5})(1223)}\right]$$
$$= 1527 \times 10^{-15} \text{ cm}^2/\text{s}$$

Equation (A) can be rewritten as

$$\operatorname{erfc}(y) = \frac{10^{17}}{3.8 \times 10^{20}} = 2.632 \times 10^{-4}$$

From the table for the erfc function in the Appendix, $y = 2.58$. Therefore, one has

$$2.58 = y = \frac{x_j}{(4Dt)^{1/2}}$$

Solving this equation for x_j yields

$$x_j = 2.58 \times (4 \times 1.527 \times 10^{-15} \times 900)^{1/2}$$
$$= 6.05 \times 10^{-6} \text{ cm} = 0.0605\ \mu\text{m}$$

The point at which $C = C_s/2$ can also be obtained from Eq. (7.18):

$$\frac{1}{2} = \operatorname{erfc}\left[\frac{x}{(4Dt)^{1/2}}\right] = \operatorname{erfc}(y)$$

Again, from the table for the erfc function, $y = 1.386$. Thus,

$$x = 1.386(4Dt)^{1/2} = 1.386(4 \times 1.527 \times 10^{-15} \times 900)^{1/2}$$
$$= 3.25 \times 10^{-6} \text{ cm} = 0.0325\ \mu\text{m}$$

Example 7.3. To form a pn junction 1.28 μm below the wafer surface in Example 7.2, a drive-in diffusion is to be carried out. Determine the doping schedule, i.e., time and temperature for the drive-in diffusion. Determine the time required for the diffusion at 1250 °C.

Solution. The amount of dopant introduced during the predeposition is given by Eq. (7.21):

$$Q_o = 2C_s\left(\frac{D_1 t_i}{\pi}\right)^{1/2} = 2 \times 3.8 \times 10^{20}\left(1.527 \times 10^{-15} \times \frac{900}{\pi}\right)^{1/2}$$
$$= 5.03 \times 10^{14} \text{ atoms/cm}^2$$

Using this value of Q_o in Eq. (7.20) for the junction 1.28 μm away, x_j yields

$$10^{17} = \frac{5.03 \times 10^{14}}{(\pi y)^{1/2}} \exp\left(-\frac{x_j^2}{4y}\right) \qquad \text{where } y = Dt$$

Solving this equation for y by trial and error gives Dt of 9×10^{-9} cm^2. Since the profile is determined entirely by Dt, a choice of temperature (and thus D) automatically yields the time. For boron diffusion at 1250°C,

$$D = 0.76 \exp\left(-\frac{3.46}{8.36 \times 10^{-5} \times 1523}\right)$$

$$= 1.193 \times 10^{-12} \text{ cm}^2/\text{s}$$

Since $Dt = 9 \times 10^{-9}$, the required time is

$$t = \frac{9 \times 10^{-9}}{D} = 7.54 \times 10^3 \text{ s} = 126 \text{ min}$$

Several cases of diffusion are of interest in introducing a dopant into a semiconductor. One such case is the predeposition from an oxide of thickness L_x having a dopant concentration of C_x that is spinned onto a semiconductor. Another is diffusion from a narrow slot of width w that would be of practical importance in shallow-diffused devices. Still another is the case in which the diffusivity is a function of time, which would result when the temperature is varied as a function of time. A similar case is one in which the diffusivity is a function of impurity concentration, which is applicable when the impurity concentration already in the semiconductor is much higher than the intrinsic carrier concentration. The expressions for the dopant profiles for these cases are summarized in Table 7.4. In the table, m is the impurity segregation coefficient at the Si-SiO$_2$ interface, which is often expressed in an Arrhenius form (Colby and Katz, 1976). For the last case, only transformed versions of the diffusion equation [Eq. (7.16)] are given, which can be solved as for Eq. (7.18) or Eq. (7.20).

Although theoretical results based on models as discussed in the previous section are available for diffusivity, particularly for the dopants for silicon, it is often necessary to determine diffusivity experimentally for specific applications. The problem is that of determining the diffusivity, given experimental measurements of the dopant profile. When experiments are carried out at constant surface concentration, the case of $D = D(C)$ in Table 7.4 applies. The transformed equation can be used to arrive at the following (see Prob. 7.11):

$$D(\beta) = -2\left[\frac{\beta C + \int_\beta^\infty C(\beta)\, d\beta}{dC/d\beta}\right] \qquad \text{where } \beta^2 = \frac{x^2}{4t} \tag{7.22}$$

Example 7.4. A doping carried out at constant surface concentration C_s for 50 minutes at 1100 K gives the following dopant profile:

TABLE 7.4
Some solutions for $C(x, t)$

Case	Solution
Diffusion from a doped oxide source†	$C(x,t) \doteq \frac{C_x(D_m/D)^{1/2}}{1+\alpha} \operatorname{erfc}\left[\frac{x}{(4Dt)^{1/2}}\right]$ where $\alpha = \frac{(D_m/D)^{1/2}}{m}$
Diffusion from a slot of width w‡	$C(r,t) \doteq \frac{Q_s w}{2\pi Dt} \exp\left(-\frac{r^2}{4Dt}\right)$ where $r^2 = x^2 + y^2 + z^2$; Q_s = surface density, atoms/cm^2
$D = D(t)$†	$\frac{\partial C}{\partial T} = \frac{\partial^2 C}{\partial x^2}$ where $T = \int_0^t D(t)\, dt$
$D = D(C)$‡	$-2\beta \frac{dC}{d\beta} = \frac{d}{d\beta}\left(D \frac{dC}{d\beta}\right)$ where $\beta^2 = \frac{x^2}{4t}$; for $C = \begin{cases} C_s & \text{at } x = 0 \ (\beta = 0) \\ 0 & \text{at } t = 0 \ (\beta = \infty) \end{cases}$ (Boundary conditions must be expressible in terms of β)
Diffusion for the initial condition; $C = C_o$ for $0 < x < h$ and $C = 0$ for $x > h$‡	$C(x,t) = \frac{C_o}{2}\left[\operatorname{erf} \frac{h-x}{(4Dt)^{1/2}} + \operatorname{erf} \frac{h+x}{(4Dt)^{1/2}}\right]$

† Ghandhi (1983).
‡ Carslaw and Jaeger (1959).

x, μm	0	0.5	1.0	1.5	2.0	...
C, cm^{-3}	9×10^{19}	5×10^{19}	7.3×10^{18}	3×10^{17}	4×10^{15}	

For the purpose of illustrating the use of Eq. (7.22), explain how D at $C = 5 \times 10^{19}$ can be determined from the above data.

Solution. A table of β versus C has to be prepared first. From the definition of β, one has

$$\beta = \frac{x}{(4t)^{1/2}} = \frac{x}{(4 \times 50 \times 60)^{1/2}} = 9.13 \times 10^{-3} x \tag{A}$$

Using Eq. (A), the data given in the table become:

β, cm/s	0	4.57×10^{-7}	9.13×10^{-7}	6.86×10^{-6}	1.83×10^{-5}
C, cm^{-3}	9×10^{19}	5×10^{19}	7.3×10^{18}	3×10^{17}	4×10^{15}

From the above table, $dC/d\beta$ at $\beta = 4.57 \times 10^{-7}$, which is for $C = 5 \times 10^{19}$, can be determined by numerical differentiation of the curve drawn from C versus β. Also, at $\beta = 4.57 \times 10^{-7}$, $\beta C = (4.57 \times 10^{-7})(5 \times 10^{19}) = 2.29 \times 10^{13}$. To evaluate the integral in Eq. (7.22), the profile should be known to the point where C is negligible. Since the complete profile is not given, let α be the integral integrated from $\beta = 4.57 \times 10^{-7}$ to the value of β at which C is negligibly small. Then, Eq. (7.22) can be written as

$$D(\beta = 4.57 \times 10^{-7}) = -2\left(\frac{2.29 \times 10^{13} + \alpha}{-9.05 \times 10^{25}}\right)$$

The diffusivity thus calculated is the value of D at $C = 5 \times 10^{19}$ cm^{-3} since the value is that at $\beta = 4.57 \times 10^{-7}$. Repeating the same procedures at various values of β yields the diffusivity as a function of C.

The diffusivity is often determined with the assumption that it is independent of concentration. In practice this is usually the case, particularly for gallium arsenide. When the diffusivity is assumed to be independent of concentration, sheet resistance measurements (e.g., Runyan, 1975) along with the surface concentration for erfc distribution [Eq. (7.18)] or Gaussian distribution [Eq. (7.20)] is sufficient to determine not only the diffusivity but also the junction depth. The sheet resistivity R_s is related to the dopant concentration as follows:

$$R_s = \frac{1}{q\int_0^{x_j} \mu C(x)\,dx} \tag{7.23}$$

where x_j is the junction depth and μ is the mobility. Average resistivity ρ is defined as

$$\rho = R_s x_j \tag{7.24}$$

Various curves such as that in Fig. 1-25 for the erfc and Gaussian distributions are available (Irvin, 1962). Given the surface concentration along with the background dopant concentration (N_B in Fig. 1-25), the average resistivity can be determined from the measured sheet resistivity as was done in Sec. 1-6. Then Eq. (7.24) yields the junction depth x_j. Once the junction depth is obtained, an estimate of the constant diffusivity can be made.

Example 7.5. Consider n-type doping by the predeposition method into a p-type semiconductor (10^{18} cm^{-3}) for 20 minutes at 1100 K. Suppose that the surface concentration is 3.1×10^{20} cm^{-3}. The sheet resistance measurement yields a value of 50 Ω. Find the junction depth x_j from Fig. 1-25. Determine the (constant) diffusivity at 1100 K.

Solution. From Fig. 1-25, the point defined by the background concentration of 10^{18} cm^{-3} and the surface concentration of 3.1×10^{20} cm^{-3} gives $R_s x_j$ of 10 μm. Therefore, the junction depth is given by

$$x_j = \frac{10}{50} = 0.2\ \mu\text{m}$$

For predeposition, the dopant profile resulting after 20 minutes at 1100 K is given by

$$C(x_j, t = 20\text{ min}) = C_s \operatorname{erfc}\left[\frac{x_j}{(4Dt)^{1/2}}\right]$$

Since the background (p-type substrate) doping level is 10^{18} cm^{-3} at $x_j = 0.2$ μm, one has

$$10^{18} = 3.1 \times 10^{20} \operatorname{erfc}(y) \qquad y = \frac{0.2 \times 10^{-4}}{(4 \times 20 \times 60 \times D)^{1/2}} = \frac{2.887 \times 10^{-7}}{D^{1/2}}$$

or $\quad \operatorname{erfc}(y) = 0.323 \times 10^{-2}$

From the table of the erfc function in the Appendix, $y = 2.08$. Therefore, the diffusivity is given by the following:

$$D^{1/2} = \frac{2.887 \times 10^{-7}}{2.08} = 1.388 \times 10^{-7}$$

$$D = 1.926 \times 10^{-14}\ \text{cm}^2/\text{s}$$

Many different methods can be used to determine the diffusivity if the dopant profile is known. For instance, two points of the profile can be used to obtain the ratio of concentrations from Eq. (7.18):

$$\frac{C_1}{C_2} = \frac{\operatorname{erfc}[x_1/(4Dt)^{1/2}]}{\operatorname{erfc}[x_2/(4Dt)^{1/2}]}$$

in which D is the only unknown, and C_1 and C_2 are the dopant concentrations at positions x_1 and x_2.

The dopant profile measurements can be made by a number of methods including the capacitance-voltage technique, the differential conductivity technique, SIMS (secondary ion mass spectroscopy), and the sheet resistance technique. For detailed diffusion studies, the SIMS method appears to be the method of choice (Tsai, 1983).

Although it is often desirable to determine the diffusivity experimentally for specific applications, many useful semi-empirical diffusivity relationships are available for silicon substrates. These are given in Fair and Tsai (1975) and Tasi *et al.* (1980) for As, Fair (1981) for P, and Fair (1981) and Ryssel *et al.* (1980) for B.

Introduction of a dopant into a semiconductor by ion implantation involves penetration of accelerated ions into the solid. As the ions penetrate the solid, the ions eventually lose their energy by collisions with the electrons and nuclei of the host material and come to rest. The manner in which the penetrating ions stop or scatter determines the dopant distribution resulting from the ion implantation. Although both elastic (simple interchange of kinetic energy with no change in the internal energies) and inelastic collisions occur with both electrons and nuclei, penetrating ions are stopped mainly by inelastic collisions with electrons (electronic stopping) and elastic collisions with nuclei (nuclear stopping) for

the energy range of interest in ion implantation (< 1 MeV). For the calculation of stopping (Townsend *et al.*, 1976), one defines cross sections for electronic and nuclear stopping S_j as follows:

$$S_j = -\frac{1}{N}\left(\frac{dE}{dx}\right)_j \qquad \text{for } j = e \text{ for electron and } n \text{ for nuclei} \tag{7.25}$$

where N is the atomic density of the target (host) atoms and dE/dx is the rate of energy loss in the direction of x. If it is assumed that the electronic stopping is independent of the nuclear stopping, it follows from Eq. (7.25) that

$$-\frac{dE}{dx} = N[S_n(E) + S_e(E)] \tag{7.26}$$

The average range R of a particle of energy E can be obtained by integrating Eq. (7.26):

$$R = \frac{1}{N}\int_0^E \frac{dE}{S_n(E) + S_e(E)} \tag{7.27}$$

The cross section for electronic stopping S_e is proportional to the square root of the energy. In some instances, the cross sections are lumped into one total cross section, which is in turn correlated to a power of E.

The total path length R in Eq. (7.27) has to be projected on the incident direction of the ion beam (Fig. 7-5) for the projected average range R_p. The depth profile of implanted ions is obtained from R_p and from the standard deviation

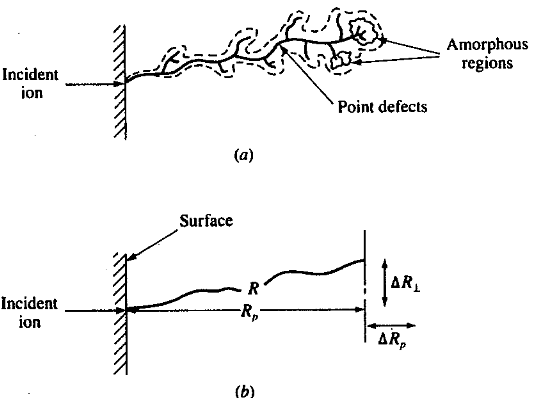

FIGURE 7-5
Disorder for typical implanted ions with corresponding ion range and straggles (ΔR_p and $\Delta R_\perp$) (Steidel, 1983).

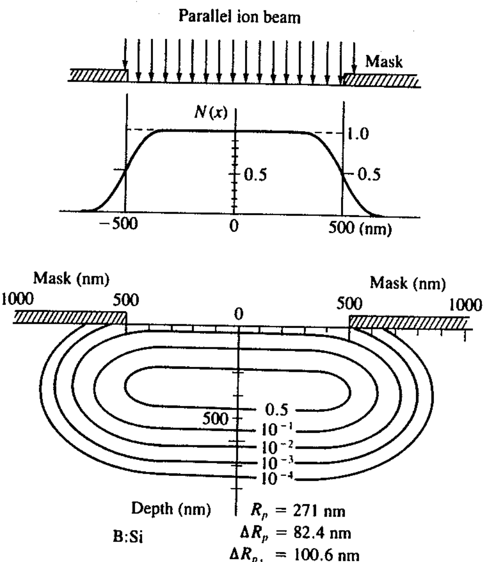

FIGURE 7-6
Contour lines of constant boron concentration after implantation through a 1-μm-wide mask and $C(x)$ at R_p (Furukawa *et al.*, 1972).

ΔR_p of a symmetric Gaussian distribution that is used to approximate the profile:

$$N(x) = \frac{N_i}{(2\pi)^{1/2}\Delta R_p}\exp\left[-\frac{(x - R_p)^2}{2\Delta R_p^2}\right] \tag{7.28}$$

where N_i is the total number of ions implanted. This profile from LSS theory (Lindhard and Scharff, 1961; Lindhard *et al.*, 1963) is derived under the assumption that Eq. (7.28) integrated from $-\infty$ to ∞ is the implanted dose (see Example 7.6). The dose N_i is obtained from the measurement of the current registered by a charge integrator connected to a metal conductor that is in good electrical contact with the wafer, and is given by

$$N_i\ (\text{atoms/cm}^2) = \frac{I\,dt}{mqA} \tag{7.29}$$

where I is the beam current (A) applied for time t (s), A is the aperture area, and m is the charge number (e.g., 1 for a singly ionized ion). Electrons pass through the integrator and neutralize the implanted charges as they come to rest in the solid. As shown in Fig. 7-5, there is also a lateral straggle $\Delta R_\perp$. If one implants through a small opening in a mask onto a semiconductor, lateral spreading cannot be ignored. In such cases, the distribution is given (Furukawa *et al.*, 1972) by

$$N(x, y) = \frac{N(x)}{(2\pi)^{1/2}\Delta R_\perp}\int_{-\infty}^{\infty}\int_{-\infty}^{\infty}\exp\left[-\frac{(y - \alpha)^2 - (d - \mu)^2}{2\Delta R_\perp^2}\right] d\alpha\, d\mu \tag{7.30}$$

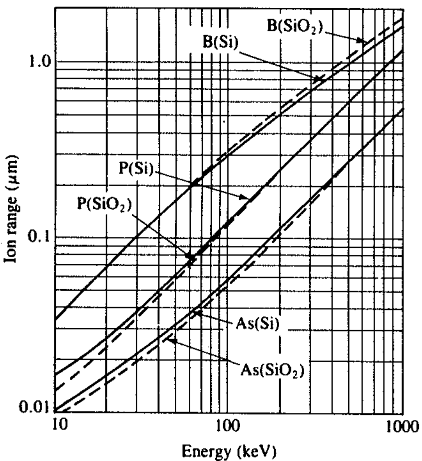

FIGURE 7-7
Projected range, R_p (Smith, 1977).

where $N(x)$ is that given by Eq. (7.28). When the mask thickness is much larger than R_p, the equation reduces to the following:

$$N(x, y) = \frac{N(x)}{2}\left[\operatorname{erfc}\left(\frac{y-a}{2^{1/2}\Delta R_\perp}\right) - \operatorname{erfc}\left(\frac{y+a}{2^{1/2}\Delta R_\perp}\right)\right] \tag{7.31}$$

where a is the half-width of the opening in the mask. An example of the lateral spread through a small opening is shown in Fig. 7-6. The values of the ion range and the ion straggles are given in Figs. 7-7 and 7-8 for typical silicon dopants. Tables of the projected range and the corresponding range straggles are given in Biersack (1981) for various substrates and dopants.

All theories on the range in a solid are based on the assumption that the target is amorphous. However, almost all semiconductors are crystalline and thus have highly anisotropic properties. Because of the ordered arrangement of lattice atoms, ions can penetrate more deeply into the crystal along major axis and planes. This phenomenon is known as the channeling effect. Within the channels along the axis and planes, no nuclear collisions (nuclear stopping) occur. The stopping takes place electronically, and the range is proportional to the ion velocity. Because of the channeling, ion implantation is often carried out with an ion beam misoriented from the major axis by an angle of at least 7 to 10°. Both silicon and gallium arsenide behave nearly as if they were amorphous solids when a misoriented beam is used. The deviations from the theoretical profile for amorphous solids that might be caused by channeling or other effects are often accounted for and approximated by the use of the "four-moment" approach (Hofker, 1975).

In many cases, ions are implanted through a layer covering the underlying semiconductor. The top layer can be a mask, an insulator, or a passivating layer.

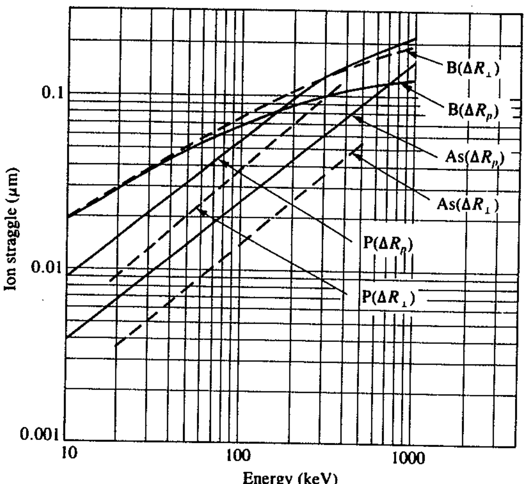

FIGURE 7-8
Calculated ion straggles, ΔR_p (vertical) and $\Delta R_\perp$ (transverse) (Smith, 1977).

If the two layers have similar ranges, they can be treated as a single layer and Eq. (7.28) applies. When they are different, the following approximation (Ishiwara *et al.*, 1975) can be used:

$$N_1 = \frac{N_i}{(2\pi)^{1/2}\Delta R_{p1}} \exp\left[-\frac{(R_{p1}-x)^2}{2\Delta R_{p1}^2}\right] \qquad 0 < x < t \tag{7.32}$$

$$N_2 = \frac{N_i}{(2\pi)^{1/2}\Delta R_{p2}} \exp\left\{-\frac{[t + (R_{p1} - t)\Delta R_{p2}/\Delta R_{p1} - x]^2}{2\Delta R_{p2}^2}\right\} \qquad x > t \tag{7.33}$$

where t is the thickness of the top layer and the subscripts 1 and 2, respectively, are for the top and bottom layer.

Example 7.6. Some characteristics of the ion distribution given by Eq. (7.28) are of interest. The position at which the implanted dopant concentration is the maximum is R_p, as can be shown by differentiating Eq. (7.28) with respect to x. The corresponding maximum concentration is given by

$$N_{\max} = \frac{N_i}{(2\pi)^{1/2}\Delta R_p} \tag{A}$$

Since both R_p and ΔR_p increase with incident ion energy, the maximum concentration decreases with increasing energy. Therefore Eq. (7.28) can also be written as

$$N(x) = N_{\max} \exp\left[-\frac{(x-R_p)^2}{2\Delta R_p^2}\right] \tag{B}$$

(*a*) Show that the amount of ion implanted that can be obtained by integrating Eq. (7.28) from zero to infinity is $N_i/2$.

(*b*) Measurements of the implanted ion profile can be used to find the parameters in Eq. (7.28). Hofker and Politiek (1980) reported the profile obtained after boron implantation into silicon at 50 keV. The dose was 10^{15} atoms/cm^2. The peak concentration was 8×10^{19} atoms/cm^3 at 0.19 μm. Determine N_i and ΔR_p from the data. Calculate $N(0)$. The experimental value of $N(0)$ was 5×10^{18} atoms/cm^3.

Solution

(*a*) The amount of ion implanted, N_T, that is obtained by integrating the equation from zero to infinity is

$$N_T = \int_0^\infty N(x)\,dx$$

$$= \frac{N_i}{(2\pi)^{1/2}\Delta R_p} \int_0^\infty \exp\left[-\frac{(x-R_p)^2}{2\Delta R_p^2}\right] dx \qquad \text{(C)}$$

Let $y = (x - R_p)/(2^{1/2}\Delta R_p)$. Then, $dx = 2^{1/2}\Delta R_p\,dy$. Therefore, Eq. (C) can be rewritten as

$$N_T = \frac{N_i}{\pi^{1/2}} \int_0^\infty \exp(-y^2)\,dy$$

$$= \frac{N_i}{2}\,\mathrm{erf}(\infty) = \frac{N_i}{2}$$

The following identities are of interest:

$$\mathrm{erf}(x) = \frac{2}{\pi^{1/2}} \int_0^x \exp(-t^2)\,dt$$

$$\mathrm{erfc}(x) = 1 - \mathrm{erf}(x)$$

$$\mathrm{erf}(\infty) = 1$$

(*b*) If the dose is 10^{15} atoms/cm^2, $N_i = 10^{15}$ atoms/cm^2. From Eq. (A),

$$N_{max} = 8 \times 10^{19}\ \text{atoms/cm}^3 = \frac{10^{15}\ \text{atoms/cm}^2}{(2\pi)^{1/2}\Delta R_p}$$

Solving this for ΔR_p yields a value of 0.05 μm. The value of $N(0)$ can be obtained from Eq. (B):

$$N(0) = N_{max} \exp\left(-\frac{R_p^2}{2\Delta R_p^2}\right)$$

$$= 8 \times 10^{19} \exp\left[-\frac{0.19^2}{2 \times (0.05)^2}\right]$$

$$= 5.9 \times 10^{16}\ \text{atoms/cm}^3$$

This calculated value of 5.9×10^{16} atoms/cm^3 compares with the experimental value of 5×10^{18} atoms/cm^3.

7.4 RADIATION DAMAGE AND ANNEALING

The crystal lattice undergoes significant structural changes as ions are bombarded into the crystal body. Atoms can be displaced from their lattice sites and the displaced atoms themselves can also displace other atoms such that a collisional cascade results. This displacement leads to the creation of vacancies and interstitial atoms, known as Frenkel defects, as well as complex lattice defects along the ion path (clusters). This damage is known as radiation damage. The damaged areas begin to overlap with increasing dose, and finally form an amorphous layer extending to a certain depth. Since the radiation damage is caused by the kinetic energy of the bombarding (penetrating) ions, it is natural that the damage is in general more severe for larger ions, higher doses, and higher energies.

Simple Frenkel defects usually result at low doses, when the ion mass is smaller than that of the target atom. These defects can have different charge states. In silicon, for instance, the defects are negatively charged in *n*-type material and neutrally charged in *p*-type material. At higher doses, locally amorphous zones, known as clusters, can form. The extent of radiation damage is also strongly dependent on implantation temperature. Significantly higher doses are required to obtain the same level of radiation damage at higher implantation temperatures. This is due to increased mobility of defects at higher temperature, which leads to a more orderly structure. In fact, the radiation damage can be cured either by subjecting the implanted substrate to a high temperature or by annealing. Thus, the implantation at high temperature corresponds to partial *in situ* annealing.

Simple defects can also lead to dislocation lines and loops. The dislocations can also result from the stress on the lattice caused by unannealed radiation damage. They can grow during annealing into undamaged regions. Dislocations anneal only at temperatures higher than 1000 °C, which is much higher than usual annealing temperatures.

Radiation damage has a significant effect on the electrical properties of semiconductors. This is not surprising in view of the fact that the electrical properties are largely determined by dopant atoms at lattice sites. Even a very small dose reduces the lifetime of charge carriers considerably. Thus, the desired electrical properties are restored only after annealing.

The total number of displaced atoms per incident ion N_d is approximately given (Kinchin and Pease, 1955) by

$$N_d = \frac{E_n}{2E_d} \qquad (7.34)$$

where E_n is the incident energy available for nuclear stopping processes (area under the $dE/dx|_n$ curve) and E_d is the displacement energy of a lattice atom, which is approximately 14 eV for silicon (Novak, 1965) and ranges from 8 to 30 eV for other semiconductors. Values of N_d are given in Table 7.5 for silicon. It is

TABLE 7.5
N_d in silicon (Kinchin and Pease, 1955)

Ion	10 keV	50 keV	700 keV
Sb	357	1785	7,143
As	357	1785	28,500
B	606	609	620
Si	357	4280	4,290

interesting to observe that N_d is the same except for the light dopant (boron) at low energies (for example, 10 keV). The range distribution of radiation damage closely follows that of implanted ion. According to Sigmund and Sanders (1967), it follows the same Gaussian distribution of Eq. (7.28) with a different range (X_D in place of R_p) and straggle (ΔX_D in place of ΔR_p). These parameter ratios are given in Fig. 7-9. One quantity of practical interest in ion implantation is the critical dose, which is the dose needed to form an amorphous layer. This critical dose for silicon is shown in Fig. 7-10 for various dopants.

Annealing accomplishes electrical activation of the implanted ions. In addition, it brings about recrystallization of the lattice. When the ionic radius of the dopant atom is very similar to that of the host atom, simultaneous activation and recrystallization can take place. However, the temperature required for the activation can be different from that for recrystallization. For gallium arsenide, for instance, radiation damage is eliminated after annealing at 500 °C. However, temperatures higher than 700 °C are necessary for the electrical activation (Ryssel and Ruge, 1986). The electrical activation is determined by Hall and sheet resistivity measurements or simply by four-point probe measurements. Details on the measurement techniques can be found in Runyan (1975).

The behavior of annealing is usually studied by two different methods. Isochronal annealing is one in which the time of annealing is held constant but the temperature is varied. Isothermal annealing is one in which the time is varied while holding the temperature constant. Annealing is mainly studied by the isochronal method. For some dopants, such as arsenic in silicon, the isochronal curve is too steep to be useful and therefore the isothermal method is used.

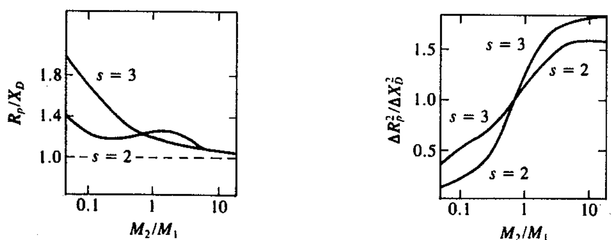

FIGURE 7-9
Ratio of R_p to radiation damage range X_D, and ratio of ΔR_p to radiation damage straggle (vertical) ΔX_D as a function of mass ratio M_2(target)/M_1(ion). A larger s corresponds to a lower energy transfer upon collision (Sigmund and Sanders, 1967).

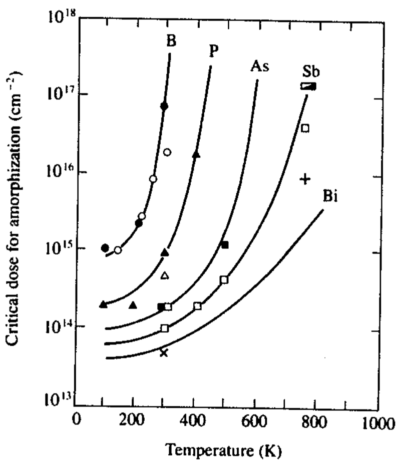

FIGURE 7-10
Critical dose for amorphization as a function of temperature (Morehead and Crowder, 1971).

Annealing for electrical activation is often described by phenomenological nth-order kinetics with respect to the electrically inactive ion concentration (e.g., Capelani *et al.*, 1974):

$$r_a = k'I^n \tag{7.35}$$

where r_a is the rate per unit volume, k' is the rate constant, and I is the concentration of electrically inactive ions. The electrically active ion concentration C is related to I as follows:

$$C(t, T) = C(0, 0) + I(0, 0) - I(t, T) \tag{7.36}$$

where $I(t, T)$ is the concentration of electrically inactive ions at time t and temperature T during annealing and $I(0, 0)$ is the same at the start of annealing. Since $C(0, 0)$ and $I(0, 0)$ constitute the sum of active and inactive ions present before annealing, the maximum possible concentration of active ions C_m is given by

$$C_m = C(0, 0) + I(0, 0) \tag{7.37}$$

Since the volume of the solid being annealed is constant, Eq. (7.35) can be rewritten as

$$\frac{dI}{dt} = kI^n \qquad \text{where } k = \frac{k'}{V} \tag{7.38}$$

and V is the volume of solid being annealed. Use of Eqs. (7.36) and (7.37) in Eq. (7.38) yields

$$\frac{dC}{dt} = -k(C_m - C)^n \tag{7.39}$$

Whether the annealing is carried out isochronally or isothermally, the temperature is constant at least for a period of time. Therefore, Eq. (7.39) can be solved as follows:

$$\ln \frac{C_m - C_o}{C_m - C} = kt \qquad \text{for } n = 1 \tag{7.40a}$$

$$(C_m - C)^{1-n} - (C_m - C_o)^{1-n} = (n-1)kt \qquad \text{for } n \neq 1 \tag{7.40b}$$

where C_o is the concentration of electrically active ions at time zero, which is much smaller than C_m and thus can be neglected.

The concentration of electrically active ions is inferred from resistivity measurements. Noting that C in Eq. (7.39) is an average concentration over a thickness to which ions are implanted, one can rewrite Eq. (7.23) as follows:

$$R_s = \frac{1}{\mu_e q x_j \left[\int_0^{x_j} C(x)\, dx / x_j \right]} = \frac{1}{\mu_e q x_j C} \tag{7.41}$$

since the quantity within the bracket is the average concentration C. In terms of average resistivity ρ [Eq. (7.24)], Eq. (7.41) becomes

$$\rho = \frac{1}{q\mu_e C} \qquad \text{or} \qquad S = q\mu_e C \tag{7.42}$$

where μ_e is an effective mobility over the thickness and S is the conductivity. Since the conductivity (inverse of ρ) is proportional to the average concentration, experimental data are often given in terms of the conductivity. The maximum concentration C_m is ideally that corresponding to the dose. However, not all implanted ions are necessarily activated by annealing. Therefore, C_m is often taken as that obtained when a plot of C versus T reaches a plateau at high temperatures.

Example 7.7. In isochronal annealing, only one sample is subjected to various temperatures but annealed for the same length of time at each temperature, and measurements are made. Let T_i and C_i be the temperature and concentration at the ith time the sample is annealed. Explain how one can determine the activation energy and preexponential factor from the isochronal annealing data.

Solution. Applying Eq. (7.40) to the intermittent annealing and measurement, one has, for instance, for first-order kinetics:

$$\ln \frac{C_m - C_{i-1}}{C_m - C_i} = k(T_i)t$$

Let the left-hand side of the above equation be Y and take the logarithm of both sides of the equation to obtain

$$\ln Y_i = -\frac{E_a}{RT_i} + \ln k_0 t \qquad \text{where } k = k_0 \exp\left(-\frac{E_a}{RT}\right)$$

Since the time is the same for all i, a plot of $\ln Y_i$ versus $1/T_i$ should yield the activation energy E_a from its slope and k_0 from the intercept. Similar procedures can be followed for $n \neq 1$. This is a form of integral kinetic analysis (e.g., Levenspiel, 1972). Therefore, various n values should be tried until a straight line (or the best fit) is obtained. For isothermal annealing, the usual procedures of Chap. 5 or those detailed in the above reference can be followed.

The annealing process is complex, as is ion implantation. An example of a complex annealing process for boron in silicon is shown in Fig. 7-11. At low doses, a slow increase in the electrical activation with temperature is seen. As the dose increases, however, a retrograde annealing (reverse annealing) results. According to Blamires (1970), the reverse annealing is due to ion-pair formation, which dissociates again at higher temperatures, and the atoms are incorporated individually into the crystal lattice. The steep increase in the electrical activation around 600 °C at high doses is usually attributed to recrystallization. Similar behavior is also observed for phosphorus in silicon, shown in Fig. 7-12. As indicated in the figure, the annealing behavior is represented by a combination of three separate reaction rates, each operative in the temperature range shown.

As device dimension and junction depth decrease, it has become necessary to activate the implanted ions in such a way that the implanted ions do not diffuse during annealing. This need has brought about rapid thermal annealing

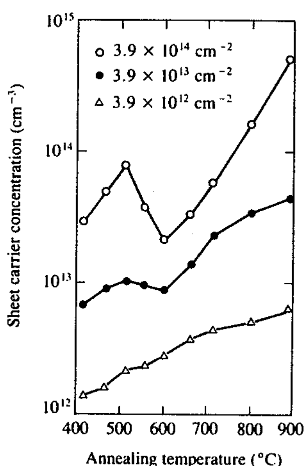

FIGURE 7-11
Isochronal annealing of boron-implanted silicon (Webber *et al.*, 1969).

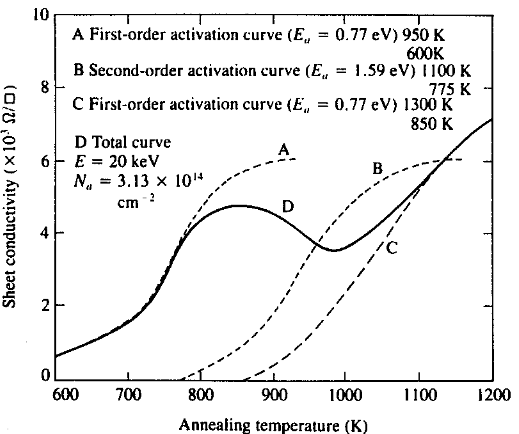

FIGURE 7-12
Isochronal annealing: sheet conductivity for phosphorus-implanted silicon (Bicknell, 1972).

(RTA) techniques. The distance S atoms travel by diffusion follows from the definition of diffusivity (Example 5.1) and is

$$S = (Dt)^{1/2} = \left[D_0 t \exp\left(-\frac{E}{k_B T}\right)\right]^{1/2} \tag{7.43}$$

where Eq. (7.2) has been used. The distance S has to be small to prevent redistribution of implanted ions by diffusion. The temperature must be set high enough to activate the electrically inactive ions, so only linked design freedom exists here. On the other hand, the time for minimum redistribution can be minimized, which is why it is called rapid annealing. It should be recognized at the same time that a certain amount of diffusion is necessary for the activation, since diffusion itself is the mechanism by which the atoms reorder their positions for activation. The distance required for the reordering might be several times the lattice constant.

Example 7.8. According to Fig. 7-12, the group of ions most difficult to activate belongs to the curve B with an activation energy of 1.59 eV, and the fraction of this group is approximately 30 percent of the total implanted ions if one uses the plateau values for each group. Determine the temperature required to activate 90 percent of the group B ions. Determine also the fraction of total ions still not activated at that temperature. Assuming that four times the silicon lattice constant is the distance for displaced atoms to diffuse for reordering of the lattice structure, calculate the (minimum) time for the annealing. The Boltzmann constant is 8.62×10^{-5} eV/K. Use the diffusivity given by $D(\text{cm}^2/\text{s}) = 0.76 \exp(-3.46/k_B T)$. The silicon lattice constant is 0.543 nm.

Solution. If the activation energy is 1.59 eV, the probable fraction of group B ions overcoming the energy barrier, f, is given by

$$f = \exp\left(-\frac{E}{k_B T}\right)$$
$$= \exp\left(-\frac{1.59}{8.62 \times 10^{-5} T}\right)$$
$$= 0.90$$

Solving this for T yields a temperature of 1.75×10^5 K. At this temperature, the fraction of group A and C ions activated is given by $\exp(-0.77/8.62 \times 1.75)$, which is 0.95. Since 90 percent of group B ions, which constitute 30 percent of the total ions, and 95 percent of groups A and C (70 percent of the total) are activated, the fraction of total ions activated, w, is given by

$$w = 0.3 \times 0.9 + 0.7 \times 0.95 = 0.935$$

Thus, 93.5 percent of the total ions are activated. The distance S the atoms have to diffuse is 4×0.543 nm = 2.172 nm. Using this value in Eq. (7.43), one has

$$2.172 \times 10^{-7}\ (\text{cm}) = \left[0.76t \exp\left(-\frac{3.46}{8.62 \times 1.75}\right)\right]^{1/2}$$

or

$$t = 7.81 \times 10^{-14}\ \text{s}$$

This example illustrates the point that the time required for the activation is very short. Although some vaporization should occur at the calculated temperature, the only limitation for rapid annealing is the ability to heat the substrate quickly. A heating method suitable for this very rapid thermal annealing is laser heating. The controllable time scale for a pulsed laser is down to 10^{-11} s, and it is 10^{-4} s for a continuous (cw) laser. The average temperature rise ΔT due to exposure to a laser beam with short wavelengths can be estimated (Bloemberger, 1979) as follows:

$$T = \frac{(1-R)I_E U}{\rho C_v (2 D_T U)^{1/2}} \tag{7.44}$$

where R is the reflectivity, C_v is the specific heat, U is the laser pulse duration, D_T is the thermal diffusivity, I_E is the pulse energy, and ρ is the density of the semiconductor. With pulsed laser annealing, melting of the surface of the irradiated semiconductor almost always occurs, followed by an epitaxial regrowth. With a cw laser, recrystallization takes place via solid phase epitaxy. Auston *et al.* (1979) expressed the regrowth rate by solid phase epitaxy as follows:

$$v = v_0 \exp\left(-\frac{E}{k_B T}\right) \tag{7.45}$$

where v_0 is 2.9×10^9 cm/s and $E = 2.7$ eV for (100) silicon. Laser annealing, while attractive, is not conducive to high throughput. Although limited in time scale (only down to 1 s), radiation heating with tungsten-halogen lamps allows arrays of wafers to be heated for annealing (Sedgewick, 1986).

During annealing, implanted atoms redistribute. If dopants do not escape out of the exposed surface during annealing, the dopant profile after annealing (Ryssel and Ruge, 1986) is given by

$$C(x, t) = \frac{N_i}{[2\pi(\Delta R_p^2 + 2Dt)]^{1/2}} \exp\left[\frac{-(x - R_p)^2}{2(\Delta R_p^2 + 2Dt)}\right]$$
$$\times \left(\frac{1}{2}\right)\left\{1 + \operatorname{erf} y_+ + \left[\exp\left(-\frac{4xR_p}{2\Delta R_p^2 + 4Dt}\right)\right](1 + \operatorname{erf} y_-)\right\} \quad (7.46)$$
$$y_\pm = \frac{R_p(4Dt)^{1/2}/(2^{1/2}\Delta R_p) \pm x(2^{1/2}\Delta R_p)/(4Dt)^{1/2}}{(2\Delta R_p^2 + 4Dt)^{1/2}}$$

Except in the immediate region near the surface, the first term before the ($\frac{1}{2}$) factor in Eq. (7.46) is sufficiently accurate for the profile. As was the case for doping by thermal diffusion, annealing is often carried out in an oxidizing environment, especially when a masking layer for the next fabrication step is to be produced simultaneously with annealing. In such cases, the dopant profile is determined by the following relationship (Prince and Schwettmann, 1974):

$$\frac{\partial C}{\partial t} = \frac{\partial}{\partial x}\left(D\frac{\partial C}{\partial x}\right) + \alpha\frac{dX}{dt}\frac{\partial C}{\partial x} \quad (7.47)$$

where the origin is at the substrate-oxide interface. Here α is the ratio of the thickness of the substrate consumed during the oxide formation to that of the oxide, which is approximately 0.44 for Si-SiO_2 (Atalla and Tannenbaum, 1960), and dX/dt is the oxide growth rate.

When a substrate is bombarded with high-energy, nondoping particles such as neutrons and protons during or after implantation, a significant increase in the rate of diffusion results. This effect is known as radiation-enhanced diffusion (Seeger and Chick, 1968; Ryssel and Ruge, 1986). Defects (vacancies in ideal cases) produced by the bombardment increase the diffusivity, since most doping elements diffuse via a vacancy mechanism. Relatively high temperatures are necessary during irradiation to avoid the formation of stable defects. In the case of silicon, the temperature must be over 750 °C.

Although not related to dopant incorporation, ion implantation damage is an effective method of gettering, as is other damage gettering such as sandblasting and sound abrasion. Gettering is a process of removing undesired impurities and defects from junction regions. Other effective gettering techniques are heavy phosphorus doping, which causes formation of ion pairs such as P^+Cu^-, and intrinsic gettering, in which oxide precipitates, such as SiO_x, play the role of a sink for capturing undesired impurities.

7.5 DOPANT REDISTRIBUTION AND AUTODOPING

After dopants are incorporated into substrates to form junctions, they undergo many processing steps for device fabrication. Although efforts are made to use

low-temperature processing techniques to minimize redistribution of incorporated dopants, the dopants still redistribute during the course of further processing. This redistribution problem can become serious enough to receive careful attention when an epitaxial film is grown on top of the doped area, because of the high temperature required for epitaxy. A consideration of this severe case of dopant redistribution leads to other dopant redistributions that can arise in various situations.

When a film is grown on a doped substrate, the dopant diffuses into the growing film in the course of the film growth. This phenomenon is referred to as autodoping (Basseches *et al.*, 1961; Srinivasan, 1980). The autodoping behavior is shown in Fig. 7-13. As shown in the figure, the dopant in the substrate diffuses out into the growing epitaxial layer, designated as Epi. At the same time, during the growth, the dopant in the substrate evaporates into the growing film. Such doping is referred to as lateral autodoping as opposed to the redistribution caused by the solid phase diffusion, called outdiffusion. It is noted that the autodoping also leads to the unintentional doping of the film in between the doped regions in Fig. 7-13, denoted as the "off" position (nondiffused area) in the figure.

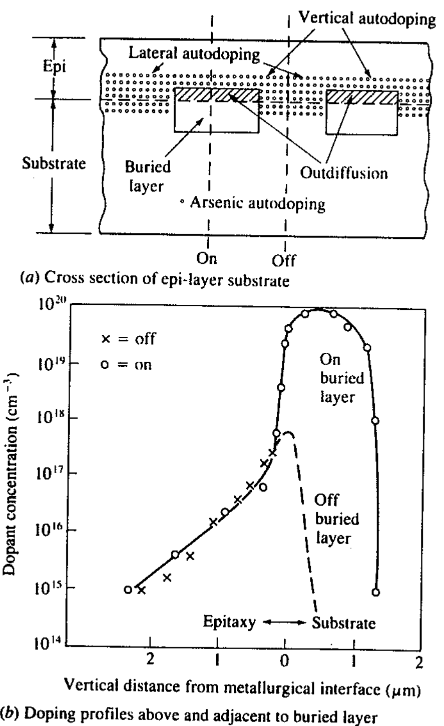

FIGURE 7-13
Autodoping effects (Srinivasan, 1980).

In the process of growing an epitaxial layer onto a substrate with a heavily doped buried layer as in BJT, the first step is to prebake the substrate so as to establish stabilized thermal and flow conditions for the epitaxial deposition to follow. This prebake is not unique to the epitaxial deposition and can represent other similar situations in fabrication steps. In this prebake, the dopant profile in the buried layer changes. Because of dopant evaporation taking place at the buried layer surface exposed to flowing gas, the dopant is carried away by the flowing gas and deposits onto the nondiffused substrate. The lateral autodoping onto the nondiffused substrate is complicated by the fact that the dopant concentration in equilibrium with the surface concentration changes with position and flow conditions. The dopant distributions resulting from the prebake are summarized in Table 7.6. The distributions are based on the assumption that the profile in the buried layer of length L is uniform at C_o initially. In the table, C_1 is the dopant profile in the buried layer, C_2 is the same in the layer below the buried layer, and C_n is the profile in the nondiffused regions. In the nondiffused regions, the profiles depend on the surface concentration of dopant in the gas phase $(C_s)_g$. Further, the surface concentration depends on the mass transport in the reactor, i.e., whether the nondiffused regions are in the upstream or downstream with respect to the position of the buried layer in the reactor. The region in the upstream is exposed to the dopant transported by gas phase diffusion only; the region in the downstream is exposed to the dopant transported by diffusion as well as convective flow. The proportionality constant α in the table is a factor relating the feed velocity U to the velocity near the substrate, which has to be chosen depending on the radial velocity profile pertinent to the flow regime.

TABLE 7.6
Dopant distribution resulting from prebake (Lee, 1986)

$$\frac{C_1}{C_o} = 0.5\,(\text{erfc}\, y_1 - \text{erfc}\, y_2) + \text{erf}\, y_3 + Y$$

$$\frac{C_2}{C_o} = 0.5\,(\text{erfc}\, y_1 - \text{erfc}\, y_4) - \text{erf}\, y_3 + Y$$

$$y_1 = (L + x)/(4Dt)^{1/2} \qquad y_2 = (L - x)/(4Dt)^{1/2}$$
$$y_3 = x/(4Dt)^{1/2} \qquad y_4 = -y_2$$
$$Y = \exp(y_5)[\text{erfc}\, y_6 - \exp(hL/D)\,\text{erfc}\, y_7]$$
$$y_5 = (hx + h^2 t)/D \qquad y_6 = y_3 + h(t/D)^{1/2}$$
$$y_7 = y_1 + h(t/D)^{1/2}$$
$$h = k_m/K_e$$

$$C_n = K_e(C_s)_g\, \text{erfc}\,[X/(4Dt)^{1/2}]$$

$$\frac{(C_s)_g}{(C_s)_b} = \begin{cases} \exp[-(a_1 - b_0)z] & \text{downstream} \\ \exp[-(a_1 + b_0)z] & \text{upstream} \end{cases}$$
$$a_1 = [(\alpha U)^2 + 4D_g k_m]/2D_g$$
$$b_0 = \alpha U/2D_g$$

After the prebake during which thermal and gas flow conditions are stabilized, reactants and dopant are introduced into the reactor for epitaxial deposition. The dopant redistribution during epitaxial deposition is distinctly different from that during the prebake in that the growing solid surface moves with time because of deposition. The one-dimensional conservation equation is

$$\frac{\partial C}{\partial t} = D\frac{\partial^2 C}{\partial x^2} \tag{7.48}$$

One of the boundary conditions is given by

$$-D\frac{\partial C}{\partial x} = k_m[(C_s)_g - C_\infty] + VC \qquad \text{at } x = x_f;\ x_f = Vt \tag{7.49}$$

where V is the constant deposition rate, x_f is the moving boundary given by Vt and C is the concentration in the bulk gas flow. It states that the flux at the moving boundary is the same as the amount transferred by mass transfer at the gas-solid interface plus the amount transferred by the deposition (Grove *et al.*, 1965). Noting that the surface concentration of the dopant in the solid, $C(0, t)$, is assumed to be in local equilibrium with the gas phase surface concentration, $(C_s)_g$, such that

$$C(0, t) = K_e(C_s)_g \tag{7.50}$$

where K_e is the equilibrium constant, Eq. (7.49) can be rewritten as

$$-D\frac{\partial C}{\partial x} = (h + V)C - k_m C \qquad \text{where } h = \frac{k_m}{K_e} \tag{7.51}$$

As shown in Fig. 7-14, the origin for the coordinate is at the epi-substrate interface. The initial condition is that resulting from the prebake. Although exact solutions are available, approximate solutions under the condition of $Vt \gg (Dt)^{1/2}$, which is usually satisfied, are useful. The approximate solutions (Lee, 1986) are

$$C(t, x) = C_i(0, x)\left(W + \frac{1 - W}{2}\,\text{erfc}\, y_3\right) \qquad \text{where } y_3 = \frac{x}{(4Dt)^{1/2}} \tag{7.52}$$

and

$$W = \frac{k_m C_\infty}{(h + V)C_o}$$

which is applicable to both diffused and nondiffused regions. It is noted, however, that $C_i(0, x)$ is C_1 in Table 7.6 for the diffused region whereas it is C_n in Table 7.6 for the nondiffused region, and that t in the equations for C_1 and C_n is the duration of the prebake, but x as used in Eq. (7.52) is applicable to the surface of the epitaxial layer. The maximum lateral autodoping, which is the maximum

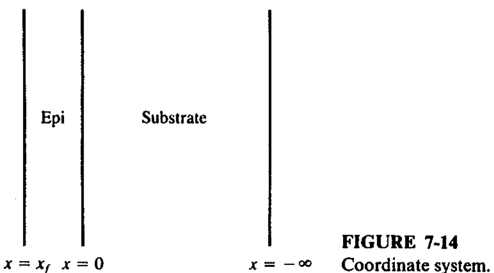

FIGURE 7-14
Coordinate system.

dopant concentration in the nondiffused region, is approximately given by

$$(C_n)_{max} = K_e(C_s)_g\left(W + \frac{1 - W}{2}\right) \tag{7.53}$$

The dopant distribution that results when no dopant is present in the feed can be obtained by simply setting C_∞ or W equal to zero. If the epitaxial layer is to be doped with an opposite type of dopant relative to the substrate, then the dopant distribution in the epitaxial layer (Grove *et al.*, 1965), C_e, is given by

$$C_e = \frac{C_f}{2}[1 + \text{erf } y_3 + \exp(z_1) \text{ erfc } (z_2)] \tag{7.54}$$

where $z_1 = (V/D)(Vt - x)$
$z_2 = (2Vt - x)/(4Dt)^{1/2}$

The corresponding dopant distribution of the opposite type, emanating from the substrate into the epitaxial layer being deposited, is given by Eq. (7.52) with $W = 0$. The junction forms at the point where $C(t, x_j) = C_e(t, x_j)$. A significant redistribution can also occur during thermal oxidation of native substrates. The distribution occurs not only due to thermal diffusion but more importantly due to segregation of dopant at the substrate-oxide interface. This segregation is represented by a segregation coefficient m (at the interface) defined as follows:

$$m = \frac{\text{equilibrium dopant concentration in substrate}}{\text{equilibrium dopant concentration in oxide}} \tag{7.55}$$

Four different cases of dopant redistribution are shown in Fig. 7-15 (Grove *et al.*, 1964). They can be considered in two groups: in one, the oxide has a tendency to take up ($m < 1$) dopant, and in the other, it has a tendency to reject ($m > 1$) dopant. In each case the situation can be different for slow and for fast diffusion in the oxide. The dopant concentration on the substrate side of the interface, $(C_s)_i$, is given (Grove *et al.*, 1964) by

$$\frac{(C_s)_i}{C_o} = \frac{1 + (C_x/C_o)\lambda}{1 + (1/m - \alpha)\pi^{1/2} \exp(\alpha^2 y_b^2) \text{ erfc } (\alpha y_b) y_b + \lambda/m} \tag{7.56}$$

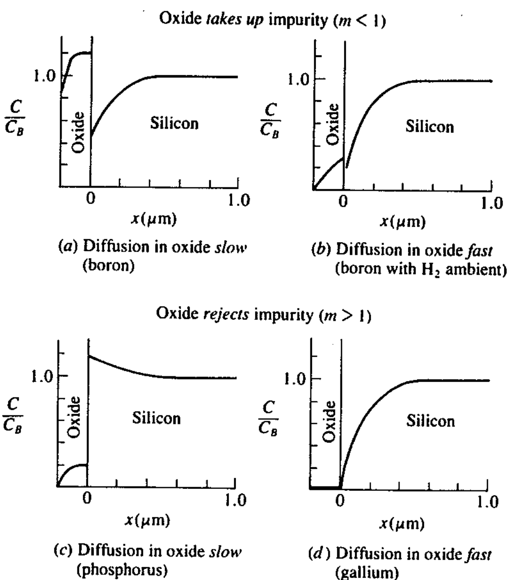

FIGURE 7-15
Four cases of impurity redistribution in silicon due to thermal oxidation (Grove *et al.*, 1964).

where $\lambda = r \exp[(\alpha^2 r^2 - 1)y_x^2] \text{ erfc } (\alpha y_b)/\text{erf } (y_x)$
$r = (D_x/D)^{1/2}$
$y_b = (B/4D)^{1/2}$
$y_x = (B/4D_x)^{1/2}$

and C_o is the initial dopant concentration in the substrate, which is assumed constant, C_x is the dopant concentration in the oxide at the gas-oxide interface, D_x is the diffusivity in the oxide, B is the parabolic rate constant (see Chap. 5, gas-solid reactions) for the oxidation, and α is the ratio of the thickness of substrate consumed during oxidation to the oxide thickness, which is 0.45 for silicon. The segregation coefficient is 10 for P, Sb, and As and 0.3 for B in Si (Grove *et al.*, 1964).

NOTATION

a	Half-width of a window (L)
A	Area (L^2)
B	Parabolic rate constant for oxidation ($L/t^{3/2}$)
C	Solid phase dopant concentration (atoms/L^3, or L^{-3})
C_m	Maximum C defined by Eq. (7.37) (atoms/L^3)

C_e	Dopant concentration in epitaxial layer given by Eq. (7.54)
C_f	Dopant concentration in gas phase
C_n	C in epitaxial layer
C_o	Constant background C in substrate
C_s	Solid surface value of C
C_v	Specific heat
C_x	C in oxide layer
C_∞	Gas phase concentration of dopant in bulk fluid flow (molecules/L^3)
$(C_i)_g$	Gas phase concentration of dopant at interface
$(C_s)_g$	Gas phase dopant concentration at solid surface
D	Diffusivity (L^2/t)
D_i	Intrinsic diffusivity
$D_i^\times, D_i^-, D_i^+$	Intrinsic diffusivity due to neutral ($\times$), negative, and positive ions
D_g	Gas phase diffusivity
D_m	Diffusivity defined by Eq. (7.14)
D_x	Diffusivity in oxide
D_T	Thermal diffusivity
D_1	Diffusivity during predeposition
E	Activation energy (E); electric field (V/L)
E_n	Incident energy available for nuclear stopping
E_d	Displacement energy of a lattice atom
h	Enhancement factor in Eq. (7.10) (dimensionless); k_m/K_e (L/t)
I	Current (I); concentration of electrically inactive ion (atoms/L^3)
I_E	Pulse energy (E)
J	Flux (molecule/L^2)
k	Rate constant
k_B	Boltzmann constant
k_m	Mass transfer coefficient (L/t)
K_e	Equilibrium constant defined in Eq. (7.50) (dimensionless)
K_{eq}	Equilibrium constant defined in Prob. 7.12
K_r	Reaction equilibrium constant
m	Charge number in Eq. (7.29); segregation coefficient defined by Eq. (7.55)
n	Electron concentration (electron/L^3 or L^{-3}); reaction order
n_i	Intrinsic value of n
N	Impurity concentration (L^{-3}) in Eq. (7.8); atomic density of target atoms in Eq. (7.25); ion concentration after implantation (L^{-3}) in Eq. (7.28)
N_i	Dose (atoms/L^2 or L^{-2})
N_0	Number of atoms displaced per incident ion
p	Hole concentration
q	Electric charge
Q_o	Total amount of dopant after predeposition (atoms/L^2)
Q_s	Surface density in Table 7.4 (atoms/L^2)

r	Radius defined in Table 7.4 (L)
R	Ion range defined by Eq. (7.27) (L); reflectivity in Eq. (7.44)
R_p	Projected value of R (L)
R_s	Sheet resistivity (Ω·cm)
ΔR_p	Standard deviation of R_p in x direction (L)
$\Delta R_\perp$	Standard deviation of R_p in y direction (L)
S	Distance atoms travel by diffusion (L)
S_e	Electronic stopping cross section (L^2E)
S_j	Quantity defined by Eq. (7.25) (L^2E)
S_n	Nuclear stopping cross section (L^2E)
t	Time (t)
t_1	Time for predeposition
T	Temperature (T)
ΔT	Temperature rise due to exposure to laser beam [Eq. (7.44)]
u	Laser pulse duration (t)
U	Bulk fluid velocity (L/t)
v	Regrowth rate given by Eq. (7.45) (L/t)
v_0	Preexponential quantity in Eq. (7.45) (L/t)
V	Epitaxial growth rate (L/t)
w	Width of a window (L)
W	Quantity defined in Eq. (7.52) (dimensionless)
x	Coordinate in the direction perpendicular to solid surface
x_j	Junction depth (L)
X	Oxide thickness (L)
y	Coordinate perpendicular to x (width coordinate)
y_1, y_2, y_3, y_4	Quantities defined in Table 7.6
Y	Quantity defined in Table 7.6
z_1, z_2	Quantities defined in Eq. (7.54)

Greek letters

α	Ratio of substrate thickness consumed during oxidation to oxide thickness; quantity defined in Table 7.4; proportionality constant in Table 7.6
β	$x/(4t)^{1/2}$
λ	Quantity defined in Eq. (7.56)
μ	Mobility (L^2/Vt)
μ_e	Effective mobility
ρ	Average resistivity (ΩL)

Units

E	Energy
I	Current
L	Length
V	Voltage

t	Time
T	Temperature
Ω	Ohm

PROBLEMS

7.1. According to Fair (1981), the diffusivities of dopants in silicon are given as follows:

$$D_{As} = 2D_i^- \frac{n}{n_i}$$

$$D_B = D_i^+ \frac{p}{n_i}$$

$$D_P = D_i^\times + D_i^{2-}\left(\frac{n}{n_i}\right)^2 \qquad \text{where } D_i^{2-} = 44.2 \exp\left(-\frac{4.37}{k_B T}\right)$$

Assuming that $n/n_i = 10^7/1.5$ and $p/n_i = 10^7/1.5$, which are also assumed to be independent of temperature, calculate the temperatures for As and P at which the diffusivities are the same as that calculated in Example 7.1 for boron. Give the dopant that is most difficult to diffuse.

7.2. When predeposition is carried out for dopant incorporation by thermal diffusion, the gas phase dopant concentration is kept constant at a high level so that the semiconductor surface is saturated with dopant. Suppose that the predeposition is carried out with phosphorus at 1040°C for 30 minutes, and the intrinsic diffusivity is 6×10^{-14} cm²/s. Calculate the amount of phosphorus incorporated through an area of 5 cm². If the predeposition is to be less than 1 percent, what would be the minimum amount of boron that has to be present initially?

7.3. Suppose that the substrate in Prob. 7.2 is already lightly doped with phosphorus at 10^{14} atoms/cm³ and that a *pn* junction is to be formed by carrying out the drive-in at the same temperature as in Prob. 7.2 at a distance 2 μm away from the surface. Determine the time required for the drive-in.

7.4. The sheet resistivity is often expressed as follows:

$$R_s = \frac{1}{q\mu_e \int_0^{x_l} C\, dx} \qquad \text{(A)}$$

where the definition of the effective mobility μ_e follows from Eq. (A) and Eq. (7.23). When the dopant surface concentration, which is approximately 2.54×10^{20} atoms/cm³ in Prob. 7.3, is much higher than the background doping (10^{14} in Prob. 7.3), the integral in Eq. (A) is approximately the same as Q_o if one excludes the background doping. Therefore, Eq. (A) can be approximated as follows:

$$R_s = \frac{1}{q\mu_e(Q_o - x_j C_B)} \qquad \text{(B)}$$

where C_B is the background dopant concentration. Note that the concentration in Eq. (A) is that for electrically active dopant, i.e., the concentration minus C_B. Suppose for the sample in Prob. 7.3 that a four-point probe measurement yields an

average resistivity of 0.02 Ω·cm. Calculate the effective hole mobility μ_e for the sample.

7.5. When the diffusivity is constant, measurements of junction depth and background doping concentration (from resistivity) are used to determine the constant diffusivity. Suppose a predeposition is carried out for 20 minutes into a background doping of 10^{16} atoms/cm³ and the junction depth is 0.5 μm for the surface dopant concentration of 10^{20} atoms/cm³. Determine the constant diffusivity.

7.6. For ion implantation of boron into silicon at 100 keV, determine the maximum ion concentration for a dose of 10^{15} cm^{-2}. Where does the maximum occur and what is the spread of ion distribution in the direction perpendicular to the incident direction compared to that in the incident direction?

7.7. Suppose that the sample in Prob. 7.6 is annealed for 30 minutes at 1000°C ($D = 10^{-13}$ cm²/s). Calculate the junction depth for a background doping of 10^{15} atoms/cm³.

7.8. For silicon, the displacement energy of a lattice atom is approximately 14 eV. Calculate the incident energy for nuclear stopping E_n for Sb using Table 7.5. Obtain a relationship between E_n and the incident energy. Your result should show that the fraction of the incident energy consumed by nuclear stopping is small. Assuming that the incident energy is entirely spent by electronic stopping, obtain a relationship for the range.

7.9. The analysis of isothermal annealing data can be carried out in the same manner as for reaction kinetics by integral or differential analysis (Levenspiel, 1972). In the annealing literature, however, a method similar to the half-life method has been used (Ryssel and Kranz, 1975). Let t_g be the time at which the electrically active ion concentration reaches g times the maximum concentration C_m. One can get a table of t_g versus temperature from various isothermal runs. From Eq. (7.40), one has

$$G_1 = kt_g; \quad G_1 = \ln\frac{1}{1-g} \qquad \text{for } n = 1 \qquad \text{(A)}$$

$$G_n = kt_g; \quad G_n = \frac{C_m^{1-n}}{n-1}\left[(1-g)^{1-n} - 1\right] \qquad \text{for } n \neq 1$$

since C_o is negligible. Equation (A) can be rewritten as

$$\ln G_i = \ln k_0 + \ln(t_g) - \frac{E}{k_B T} \qquad \text{for } i = 1 \text{ or } n$$

or

$$\ln(t_g) = \ln\left(\frac{k_0}{G_i}\right) - \frac{E}{k_B T} \qquad \text{(B)}$$

According to Eq. (B), a plot of ln (t_g) versus $1/T$ should give the activation energy from the slope. Ryssel and Kranz (1975) gave the following data for the annealing of As in Si for $g = 0.9$:

t_g, min	23	205	1000
1000/T, K^{-1}	1.315	1.385	1.426

Determine the activation energy. Discuss ways of determining the order n.

7.10. According to Yeh and Armstrong (1961), the surface concentration of boron in silicon is 2.5×10^{20} atoms/cm^3 when the substrate is exposed to a B_2O_3 partial pressure of 0.01 torr at 1100 °C in the region where Henry's law applies. According to our definition of K_e, we have

$$C_s = K_e(C_s)_g$$

Determine the equilibrium constant K_e. Typical values of k_m and epitaxial growth rate are 5 cm/s and 1 μm/min, respectively. Determine the dopant concentration in the bulk gas flow that will make W in Eq. (7.52) larger than 0.1. Assume that the initial concentration in the substrate is 10^{16} atoms/cm^3.

7.11. For the dopant, the profile resulting from a predeposition can be written as follows:

$$-2\beta \frac{dC}{d\beta} = \frac{d}{d\beta}\left(D \frac{dC}{d\beta}\right) \qquad \text{(A)}$$

which is the fourth entry in Table 7.4. Derive Eq. (7.22) from Eq. (A).

7.12. Only a fraction of implanted ions is activated by annealing unless the ion dose is low (e.g., less than 10^{16} cm^{-2} for As in Si) or the annealing temperature is high (e.g., greater than 1000 °C). According to the model proposed by Tsai *et al.* (1980), arsenic atoms form clusters of three atoms that are partially active when the concentration is larger than 10^{20} cm^{-3}. Relationships for the clusters are proposed as follows:

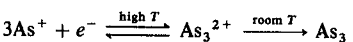

$$3As^+ + e^- \underset{}{\overset{\text{high } T}{\rightleftharpoons}} As_3^{2+} \xrightarrow{\text{room } T} As_3 \qquad \text{(A)}$$

The equilibrium for the first path is

$$K_{eq} = \frac{[As_3^{2+}]}{n[As^+]^3} \qquad \text{(B)}$$

The carrier concentration at the annealing temperature is

$$n = [As^+] + 2[As_3^{2+}] \qquad \text{(C)}$$

The equilibrium constant K_{eq} is given by

$$K_{eq} = 1.26 \times 10^{-70} \exp\left[\frac{2.06(\text{eV})}{kT}\right] \qquad \text{(D)}$$

Show that the total amount of ions implanted per unit volume N_v is given by

$$N_v = x + \frac{3K_{eq}X^4}{1 - 2K_{eq}X^3} \qquad \text{(E)}$$

where X is the concentration of As^+. For N_v of 1.84×10^{20} atoms/cm^3, calculate $[As^+]$ at 800 and 1000 °C.

REFERENCES

Attala, M. M., and E. Tannenbaum: *Bell Syst. Tech. J.*, vol. 39, p. 933, 1960.

Auston, D. H., J. A. Golovhenko, A. L. Simons, R. E. Shlusher, P. R. Smith, C. M. Surco, and T. N. C. Venkatesan: in S. D. Ferris, H. J. Leamy, and J. M. Poate (eds.), *Laser Solid Interactions and Laser Processing 1978*, p. 11, American Institute of Physics, New York, 1979.

Basseches, H., R. C. Manz, C. O. Thomas, and S. K. Tung: in J. B. Schroeder (ed.), *AIME Semiconductor Metallurgy Conference, LA*, vol. 15, Interscience Publishers, New York, 1961.

Bicknell, R. W.: *Phil. Mag.*, vol. 26, p. 273, 1972.

Biersack, J. P.: *Nucl. Inst. Heth.*, vol. 182/183, p. 199, 1981.

Blamires, N. G.: *European Conference on Ion Implantation*, p. 52, Reading, Stevenage, England, 1970.

Bloemberger, N.: in S. D. Ferris, H. J. Leamy, and J. M. Poate (eds.), *Laser Solid Interactions and Laser Processing 1978*, p. 52, American Institute of Physics, New York, 1979.

Boltaks, B. J.: *Diffusion in Semiconductors*, Academic Press, New York, 1963.

Cappelani, F., G. Restelli, and I. Spinoni: *J. Phys. C.: Solid State Phys.*, vol. 1, p. 650, 1974.

Carslaw, H. S., and J. C. Jaeger: *Conduction of Heat in Solids*, Oxford University Press, 1959.

Colby, J. W., and L. E. Katz: *J. Electrochem. Soc.*, vol. 123, p. 409, 1976.

Fair, R. B.: in F. F. Y. Wang (ed.), *Impurity Doping Processes in Silicon*, North-Holland, New York, 1981.

——— and J. C. C. Tsai: *J. Electrochem. Soc.*, vol. 122, p. 1689, 1975.

Frank, W., U. Gosele, H. Mehrer, and A. Seager: in G. E. Murch and A. S. Nowick (eds.), *Diffusion in Crystalline Solids*, chap. 2, Academic Press, New York, 1984.

Furukawa, S., H. Matsumura, and H. Ishiwara: *Jap. J. Appl. Phys.*, vol. 11, p. 134, 1972.

Ghandhi, S. K.: *VLSI Fabrication Principles*, Wiley-Interscience, New York, 1983.

——— and R. J. Field: *Appl. Phys. Lett.*, vol. 38, p. 267, 1981.

Gibbon, C. F., E. J. Povilonis, and D. R. Ketchow: *J. Electrochem. Soc.*, vol. 119, p. 767, 1972.

Gise, P. E., and R. Blanchard: *Semiconductor and Integrated Circuit Fabrication Techniques*, Reston Publishing Company, Reston, Va., 1979.

Grove, A. S., O. Leistiko, and C. T. Sah: *J. Appl. Phys.*, vol. 35, p. 2695, 1964.

———, A. Roder, and C. T. Sah: *J. Appl. Phys.*, vol. 36, p. 802, 1965.

Hofker, W. K.: Phillips Research Reports Supplement 8, 1975.

——— and J. Politiek: *Philips Tech. Rev.*, vol. 39, p. 1, 1980.

Hu, S. M., and S. Schmidt: *J. Appl. Phys.*, vol. 39, p. 4272, 1968.

Irvin, J. C.: *Bell Syst. Tech. J.*, vol. 41, p. 387, 1962.

Ishiwara, H., S. Furukawa, J. Yamada, and M. Kawamura: in S. Namba (ed.), *Proceedings on Ion Implantation in Semiconductors*, Plenum Press, New York, 1975.

Kennedy, D. P., and R. R. O'Brien: *IBM J. Res. Dev.*, vol. 9, p. 3, 1965.

Kinchin, G. H., and R. S. Pease: *Rep. Prog. Phys.*, vol. 18, p. 1, 1955.

Lee, H. H.: *J. Electrochem. Soc.*, vol. 133, p. 2416, 1986.

Levenspiel, O.: *Chemical Reaction Engineering*, 2d ed., Wiley, New York, 1972.

Lin, A. M. R., D. A. Antoniadis, and R. W. Dutton: *J. Electrochem. Soc.*, vol. 128, p. 1131, 1981.

Lindhard, J., and H. Scharff: *Phys. Rev.*, vol. 124, p. 128, 1961.

———, M. Scharff, and H. Schiott: *Kgl. Dan. Vidensk. Selsk. Mat.-Fys. Medd.*, vol. 33, p. 14, 1963.

Morehead, F. F., and B. L. Crowder: in F. H. Eisen and L. T. Chadderton (eds.), *First International Conference on Ion Implantation, Thousand Oaks*, Gordon and Breach, New York, 1971.

Novak, R. L.: *Bull. Am. Phys. Soc.*, vol. 8, p. 235, 1965.

Prince, J. L., and F. N. Schwettmann: *J. Electrochem. Soc.*, vol. 121, p. 705, 1974.

Runyan, W. R.: *Semiconductor Measurements and Instrumentation*, McGraw-Hill, New York, 1975.

Ryssel, H., and H. Kranz: *Appl. Phys.*, vol. 7, p. 11, 1975.

——— and I. Ruge: *Ion Implantation*, Wiley-Interscience, New York, 1986.

———, K. Muller, K. Haberger, R. Henkelmann, and F. Jahael: *Appl. Phys.*, vol. 22, p. 35, 1980.

Seeger, A., and K. P. Chick: *Phys. Stat. Sol.*, vol. 29, p. 455, 1968.

Sedgewick, T.: *Reduced Temperature Processing for VLSI*, p. 49, The Electrochemical Society, Pennington, N.J., 1986.

Steidel, T. E.: in S. M. Sze (ed.), *VLSI Technology*, chap. 6, McGraw-Hill, New York, 1983.

Shaw, D. (ed.): *Atomic Diffusion in Semiconductor*, Plenum, New York, 1973.

Sigmund, P., and J. B. Sanders: in P. Glotin (ed.), *Proceedings of International Conference on Applied Ion Beams Semiconductor Technology*, p. 215, Grenoble, 1967.

Smith, B.: "Ion Implantation Range Data for Silicon and Germanium Development Technology," Research Studies, Forest Grove, Oregon, 1977.

Srinivasan, G. R.: *J. Electrochem. Soc.*, vol. 127, p. 1334, 1980.
Taniguchi, K., Kurosawa, and M. Kashiwagi: *J. Electrochem. Soc.*, vol. 127, p. 2243, 1980.
Townsend, P. D., J. C. Kelly, and N. E. W. Hartly: *Ion Implantation, Sputtering and Their Applications*, Academic Press, 1976.
Tsai, J. C. C.: in S. M. Sze (ed.), *VLSI Technology*, chap. 5, McGraw-Hill, New York, 1983.
———, F. F. Morehead, and J. E. E. Baglin: *J. Appl. Phys.*, vol. 51, p. 3230, 1980.
Tuck, B.: *Introduction to Diffusion in Semiconductors*, vol. 16, p. 119, IEE Monograph Services, London, 1974.
Webber, R. F., R. S. Thorm, and L. N. Large: *Int. J. Electronics*, vol. 26, p. 163, 1969.
Yeh, T. H., and W. Armstrong: Electrochemical Society Meeting, Abstract 69, Indianapolis, Spring 1961.

CHAPTER 8

PATTERN GENERATION, TRANSFER, AND DELINEATION

8.1 LITHOGRAPHY

Design of an integrated circuit eventually leads to specification of the circuit elements in terms of the length, width, and depth of each element such as doped regions, isolated (insulated) regions, conducting regions, and so on. The "blueprint" containing the specifications and the layout of the device elements is referred to as composite layout. Elements overlay in the device structures considered in Chap. 1 (e.g., Fig. 1-13), so it is necessary to specify the order that overlaying elements are to be processed for device fabrication and also specify the patterns of the layout corresponding to each step of the fabrication.

The minimum number of patterns required for fabrication is the number of mask levels. Each level represents the mask that can be used to transfer the mask pattern to the wafer surface. Figure 8-1 shows a composite layout of a minimum geometry bipolar transistor (Colclaser, 1980). The corresponding mask levels are shown in Fig. 8-2 in the order to be fabricated. Note that the first mask level is for the mask defining the pattern for the buried layer, although the dimensions are not given. The masks in Fig. 8-2 are to the scale of the composite layout in Fig. 8-1. The second mask is for isolating the buried layer from the rest of the device structure to be fabricated by subsequent processing. An examination of all